

Reexamining the neutron skin thickness within a density dependent hadronic model

S.S. Avancini,¹ J.R. Marinelli,¹ D.P. Menezes,¹ M.M.W. Moraes,¹ and A.S. Schneider¹

¹*Depto de Física - CFM - Universidade Federal de Santa Catarina Florianópolis - SC - CP. 476 - CEP 88.040 - 900 - Brazil*

In the present work we calculate the ^{208}Pb neutron skin thickness, binding energy, surface energy and density profiles within the Dirac solution of a density dependent hadronic model. The same calculation is performed with the NL3 parametrization of the non-linear Walecka model. The asymmetry of a polarized electron scattered from a heavy target is also obtained within a partial wave expansion calculation. The theoretical results are then ready to be compared with the experimental results expected to be available very soon at the Jefferson Laboratory. For completeness, other nuclei as ^{40}Ca , ^{48}Ca , ^{66}Ni and ^{90}Zr are also investigated.

PACS number(s): 21.65.+f, 24.10.Jv, 95.30.Tg, 26.60.+c

I. INTRODUCTION

Relativistic models are a very useful tool in the description of a wide variety of applications in nuclear matter, finite nuclei and nuclear astrophysics. They can be tested and, hopefully constrained, according to experimental and astrophysical observation results. Unfortunately, most theoretical results are model dependent and so far it is unclear whether some of them should be discarded. Many variations of the well known quantum hydrodynamic model [1] have been developed and used along the last decades. Some of them rely on density dependent couplings between the baryons and the mesons [2, 3, 4, 5] while others use constant couplings [6, 7, 8]. Still another possibility of including density dependence on the Lagrangian density is through the coupling of the mediator mesons among themselves [9]. The strong model dependence of the results come from the simple fact that relativistic model couplings are adjusted in order to fit expected nuclei properties such as binding energy, saturation density, compressibility and energy symmetry at saturation density only. Once the same relativistic models are extrapolated to higher densities as in stellar matter or higher temperatures as in heavy-ion collisions or even to lower densities as in the nuclear matter liquid gas phase transitions, they can and indeed provide different information. Hence, experimental constraints obtained either from polarized electron scattered from a heavy target, from heavy-ion collisions at different energies or from astronomical observations are very important in order that adequate models are chosen and inadequate ones are ruled out.

In the present work we focus our attention to the calculation of the difference between the neutron and the proton radii known as the neutron skin thickness. Based on the argument that experimental results should be used to constrain relativistic models, it is very important that an accurate experimental measurement of the neutron skin thickness is achieved. This depends on a precise measurement of both the charge and the neutron radius.

The charge radius is already known within a precision of one percent for most stable nuclei, using the well-known single-arm and non-polarized elastic electron scattering technique as well as the spectroscopy of muonic atoms [10]. For the neutron radius, our present knowledge has an uncertainty of about 0.2 fm [11]. However, using polarized electron beams it is possible to obtain the neutron distribution, as first discussed in [12] and, as a consequence, to obtain the desired neutron radius. In fact, the Parity Radius Experiment (PREX) at the Jefferson Laboratory [13] is currently running to measure the ^{208}Pb neutron radius with an accuracy of less than 0.05 fm, using polarized electron scattering. In the PREX experiment, the asymmetry is expected to be measured at a momentum transfer $q \approx 0.4 \text{ fm}^{-1}$.

At this point it is worth mentioning that two other experimental methods have been used in order to measure neutron skins and neutron halos [14, 15], namely, the nuclear spectroscopy analysis of the antiproton annihilation residues one mass unit lighter than the target mass and the measurements of strong-interaction effects on anti-protonic X rays. Whenever possible, the results obtained with the above mentioned methods are also used for comparison in the results section.

In a recent work [16], the neutron skin thickness and the asymmetry for polarized electron scattering off a hadronic target were investigated with the help of both density dependent and with constant coupling relativistic models. For these calculations two important compromises were made: for the calculation of the proton and neutron densities, a Thomas-Fermi approach was used and for the calculation of the asymmetry a Plane Wave Born Approximation for the electron [17] was enforced. The ^{208}Pb neutron skin thickness was then obtained with two different density dependent hadronic (DDH) model parametrizations, the TW [3], where the density dependence is introduced explicitly through the couplings and the NL $\omega\rho$ model [9], where the density dependence appears through the coupling of the vector and the isovector mesons. One of the most used parametrizations of the non-linear Walecka model (NLWM), the NL3 was also used. The asymmetry, in the momentum transfer range of interest for the calculation of neutron skins, was shown to give very similar results for all models. On the other hand, the neutron skin thickness is smaller with

the DDH model than with the NL3. As the coupling strength between the ω and ρ mesons increases in the NL $\omega\rho$ model, the neutron skin thickness moves from the original NL3 towards the DDH results. As the momentum transfer increases, the asymmetry becomes strongly model dependent.

In the present work we revisit the same quantities, but with improvements in both approximations mentioned above in order to check if the model differences remain. As the target is a heavy nucleus (^{208}Pb), the results for the asymmetry are reconsidered with the use of the partial wave expansion method as briefly discussed in the Appendix. On the other hand, the proton and neutron densities are calculated from the solution of the Dirac equation. We also extend our calculations to obtain the neutron skin thickness of ^{40}Ca , ^{48}Ca , ^{66}Ni and ^{90}Zr . For the asymmetry, we also include applications for ^{48}Ca . As the NL $\omega\rho$ model was shown to give results that interpolate between the NL3 parametrization of the NLWM and the TW parametrization of the DDH model, we next restrict ourselves to the NL3 and the DDH models, i.e., one with constant couplings and another one with density dependent couplings. We also comment on the differences between the results obtained in the present work and within the Thomas-Fermi approximation. It is worth mentioning that most applications to neutron stars, to equations of state used to describe supernova simulations and the description of nucleation processes have been done within the Thomas-Fermi approximation. Understanding its limitations and accuracy is indeed very important. Information about the skin thickness as obtained in finite nuclei can be directly related to astrophysical calculations and so the possible connections between Thomas-Fermi and Dirac density profiles can be useful.

The paper is organized as follows: in section II we show the Lagrangian density of the DDH model and describe the formalism used; in section III we present and discuss the results; in section IV we draw our final conclusions.

II. FORMALISM

We describe the main quantities of the DDH model, which has density dependent coupling parameters in the following. The Lagrangian density reads:

$$\begin{aligned} \mathcal{L}_H = & \bar{\psi} \left[\gamma_\mu \left(i\partial^\mu - \Gamma_v V^\mu - \frac{\Gamma_\rho}{2} \boldsymbol{\tau} \cdot \mathbf{b}^\mu \right. \right. \\ & \left. \left. - e \frac{(1 + \tau_3)}{2} A^\mu \right) - (M - \Gamma_s \phi) \right] \psi \\ & + \frac{1}{2} (\partial_\mu \phi \partial^\mu \phi - m_s^2 \phi^2) - \frac{1}{4} \Omega_{\mu\nu} \Omega^{\mu\nu} \\ & + \frac{1}{2} m_v^2 V_\mu V^\mu - \frac{1}{4} \mathbf{B}_{\mu\nu} \cdot \mathbf{B}^{\mu\nu} + \frac{1}{2} m_\rho^2 \mathbf{b}_\mu \cdot \mathbf{b}^\mu - \frac{1}{4} F_{\mu\nu} F^{\mu\nu} \quad (1) \end{aligned}$$

where ϕ , V^μ , \mathbf{b}^μ and A^μ are the scalar-isoscalar, vector-isoscalar and vector-isovector meson fields and the photon field respectively, $\Omega_{\mu\nu} = \partial_\mu V_\nu - \partial_\nu V_\mu$, $\mathbf{B}_{\mu\nu} = \partial_\mu \mathbf{b}_\nu - \partial_\nu \mathbf{b}_\mu - \Gamma_\rho (\mathbf{b}_\mu \times \mathbf{b}_\nu)$, $F_{\mu\nu} = \partial_\mu A_\nu - \partial_\nu A_\mu$ and $\tau_3 = \pm 1$ for protons and neutrons respectively. The parameters of the model are: the nucleon mass $M = 939$ MeV, the masses of the mesons m_s , m_v , m_ρ , the electromagnetic coupling constant $e = \sqrt{4\pi/137}$ and the density dependent couplings Γ_s , Γ_v and Γ_ρ , which are adjusted in order to reproduce some of the nuclear matter bulk properties, using the following parametrization:

$$\Gamma_i(\rho) = \Gamma_i(\rho_{sat}) h_i(x), \quad x = \rho/\rho_{sat}, \quad (2)$$

with

$$h_i(x) = a_i \frac{1 + b_i(x + d_i)^2}{1 + c_i(x + d_i)^2}, \quad i = s, v \quad (3)$$

and

$$h_\rho(x) = \exp[-a_\rho(x - 1)], \quad (4)$$

with the values of the parameters m_i , $\Gamma_i(\rho_{sat})$, a_i , b_i , c_i and d_i , $i = s, v, \rho$ given in [3]. This model does not include self-interaction terms for the meson fields as in NL3. We consider two parametrizations of the above mentioned DDH model, the original one that we next refer to as TW and a more recent one known as DDME1 [18], obtained from a fitting that includes known experimental values of the ^{208}Pb neutron skin.

Once the Lagrangian density is chosen, the Euler-Lagrange equations are used to calculate the equations of motion. The meson field equations of motion are easily found in the literature and we refrain from writing them. An interested reader can obtain the equations in [2, 3, 16, 20], among other papers in the literature.

The Dirac equation for the nucleon field reads:

$$[\gamma^\mu (i\partial_\mu - \Sigma_\mu) - (M - \Sigma_s)] \Psi = 0, \quad (5)$$

where the scalar and vector self-energies are given respectively by

$$\Sigma_s = \Gamma_s \phi, \quad \Sigma_\mu = \Sigma_\mu^{(0)} + \Sigma_\mu^R, \quad (6)$$

with

$$\Sigma_\mu^{(0)} = \Gamma_v V_\mu + \frac{\Gamma_\rho}{2} \vec{\tau} \cdot \mathbf{b}_\mu + e \frac{(1 + \tau_3)}{2} A_\mu, \quad (7)$$

$$\Sigma_\mu^R = \frac{j_\mu}{\rho} \left(\frac{\partial \Gamma_v}{\partial \rho} \bar{\psi} \gamma^\nu \psi V_\nu + \frac{1}{2} \frac{\partial \Gamma_\rho}{\partial \rho} \bar{\psi} \gamma^\nu \vec{\tau} \psi \cdot \mathbf{b}_\nu - \frac{\partial \Gamma_s}{\partial \rho} \bar{\psi} \psi \phi \right).$$

The term Σ_μ^R is known as the rearrangement term. As done in [1, 19], we consider that the nucleus is approximately given by a Slater determinant and only the lowest lying positive energy states are occupied. The usual ansatz for the nucleon spinor is

$$\psi(\vec{r}, t) = \psi(\vec{r}) \exp(-iEt), \quad (8)$$

and the one-particle states are obtained from the solution of the Dirac equation. Only spherically symmetric nuclei are considered and the usual notation for the expected values of the meson fields are used. The self-energies become:

$$\Sigma_0 = \Gamma_v V_0(r) + \frac{1}{2} \Gamma_\rho \tau_3 b_0(r) + e \frac{(1 + \tau_3)}{2} A_0(r) + \Sigma_0^R, \quad (9)$$

$$\Sigma_0^R = \left(\frac{\partial \Gamma_v}{\partial \rho} \rho(r) V_0 + \frac{1}{2} \frac{\partial \Gamma_\rho}{\partial \rho} \rho_3(r) b_0 - \frac{\partial \Gamma_s}{\partial \rho} \rho_s(r) \phi \right), \quad (10)$$

where $\rho_3 = \rho_p - \rho_n$ and ρ_s and ρ are the usual scalar and baryonic densities. Next the ansatz given in eq.(8) and the spin-isospin wavefunctions $\psi = \begin{pmatrix} g_\kappa(r) \mathcal{Y}_\kappa^{jm} \\ i f_\kappa(r) \mathcal{Y}_{-\kappa}^{jm} \end{pmatrix} \otimes \xi$ are substituted into the Dirac equation. $\mathcal{Y}_{\pm\kappa}^{jm}$ and ξ are the spinorial spherical harmonics and the isospin wavefunctions respectively. After some straightforward algebraic manipulations, a new system of coupled equations is obtained:

$$(M^*(r) + V(r)) g_\kappa(r) - \left(\frac{\partial}{\partial r} - \frac{\kappa - 1}{r} \right) f_\kappa(r) = E g_\kappa(r)$$

$$\left(\frac{\partial}{\partial r} + \frac{\kappa + 1}{r} \right) g_\kappa(r) - (M^*(r) - V(r)) f_\kappa(r) = E f_\kappa(r), \quad (11)$$

where

$$M^*(r) = M - \Gamma_s(r) \phi(r),$$

and

$$V(r) = \Gamma_v(r) V_0(r) + \frac{\Gamma_\rho(r)}{2} \tau_3 b_0(r) + e \frac{(1 + \tau_3)}{2} A_0(r) + \Sigma_0^R(r).$$

At this point, $f_\kappa(r)$ and $g_\kappa(r)$ are expanded in the harmonic oscillator basis of dimensions N and M respectively, as in [19]. The linear variational method is then used to solve the above equations and we are left with an eigenvalue problem solved by the diagonalization of a matrix of order $N + M$. The fields ϕ , V_0 and b_0 are also expanded in a harmonic oscillator basis and solved iteratively through their corresponding Klein-Gordon equations. The Coulomb field A_0 is obtained by the Green's function method.

The proton and neutron mean-square radius are defined as

$$R_i^2 = \frac{\int d^3r r^2 \rho_i(\mathbf{r})}{\int d^3r \rho_i(\mathbf{r})}, \quad i = p, n \quad (12)$$

and the neutron skin thickness reads

$$\theta = R_n - R_p. \quad (13)$$

It is also useful to define the nuclear charge distribution as:

$$\rho_c(\vec{r}) = \frac{1}{[(a_p^2 - B^2)\pi]^{3/2}} \int d^3r' \exp\left[-\frac{(\vec{r} - \vec{r}')^2}{(a_p^2 - B^2)}\right] \rho_p(\vec{r}'), \quad (14)$$

where $B^2 = b^2/A$, $a_p = 0.653$ fm and b is the oscillator length used to define our basis set. The above definition includes the proton finite size, for which we have assumed a gaussian shape to describe its intrinsic charge distribution:

$$\rho_{int}(r) = \frac{1}{(a_p^2 \pi)^{3/2}} \exp(-r^2/a_p^2), \quad (15)$$

and an approximate center-of-mass correction according to the prescription given in [21]. Neutron finite size corrections are disregarded, i.e., its intrinsic form factor is taken as unit.

For the calculation of the differential elastic electron cross-section ($\frac{d\sigma}{d\Omega}$) and the asymmetry (\mathcal{A}), details are given in the Appendix.

III. RESULTS AND DISCUSSION

We first plot the ^{208}Pb neutron and proton densities obtained for the DDH model within the Thomas-Fermi approximation from [16] and the solution of the Dirac equation in Fig. 1. As it is well known, the Thomas-Fermi approximation flattens the central energy densities while the Dirac equation keeps the internal nuclear structure. The difference in the central density is then compensated near the surface, with consequences in the calculations of the mean square radii and neutron skin thickness. One can see that the DDME1 parametrization gives almost the same density profiles as compared with the original TW parametrization.

In table I we show the results of the present calculations for ^{208}Pb obtained with the NL3 and both

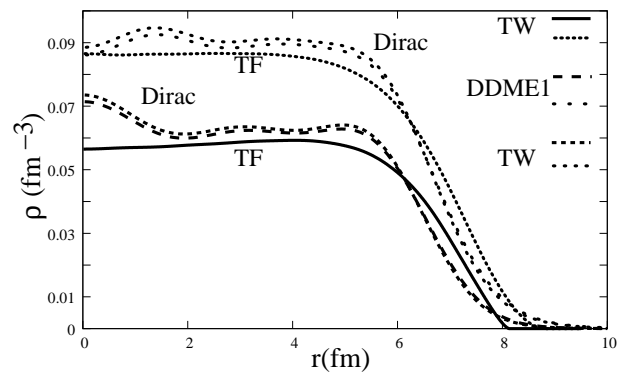


FIG. 1: ^{208}Pb neutron and proton densities obtained with TW (Thomas-Fermi), DDME1 (Dirac) and TW (Dirac). Larger densities are for neutrons and lower for protons.

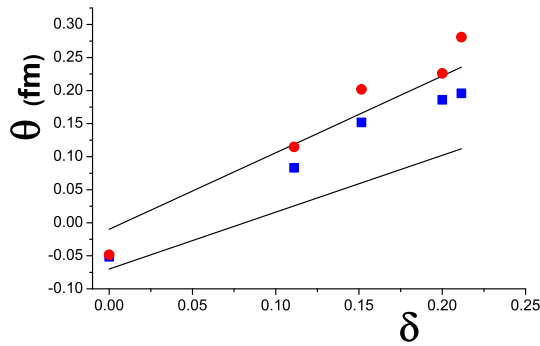


FIG. 2: Skin thickness as a function of the proton-neutron number asymmetry. Squares represent our values in the TW and full circles in the NL3. The lines represent the limits for the fitting given in [14]. From lower to higher asymmetries we have plotted the results for ^{40}Ca , ^{90}Zr , ^{66}Ni , ^{48}Ca and ^{208}Pb .

parametrizations of the DDH model. For the sake of completeness we also include the results obtained in [16] within the Thomas-Fermi approach. One can observe that the Thomas-Fermi results for the radii are systematically larger than the Dirac solutions, but the neutron skins are smaller. The surface energies also give smaller contributions within the TF approach. Both parametrizations of the DDH model show the same neutron skins albeit the small differences in the proton and neutron radii. The binding energy and the surface energy are also slightly different. Finally, the charge radius (R_c), calculated with the charge distribution given by equation (14) is presented and compared with the experimental value. All results are very similar.

In table II we show the results for ^{40}Ca , ^{48}Ca , ^{66}Ni and ^{90}Zr . Most of the conclusions drawn from Table I remain valid, i.e., the neutron skin thickness are the same for both parametrizations of the DDH model, TW gives larger surface energies than DDME1 and NL3 and the proton, neutron and charge radii vary from one model to the other.

According to [14], experimental data show a linear relation between the neutron skin thickness and the proton-neutron asymmetry of the considered nuclei, i.e., $\delta = (N - Z)/A$. Assuming that this dependence really exists, the authors of [14] fit it as

$$\theta = (-0.04 \pm 0.03) + (1.01 \pm 0.15)\delta. \quad (16)$$

In Fig. 2 we have plotted the fitted dependence lines considering the most extreme values for θ . If this dependence has really to be satisfied, the theoretical points should lie within both curves. The TW and DDME1 points coincide and they are shown to be inside the appropriate range while the NL3 results for very asymmetric nuclei are outside the upper boundary.

Now let's focus on the electron scattering cross sections and the asymmetry. In Fig. 3 the elastic cross

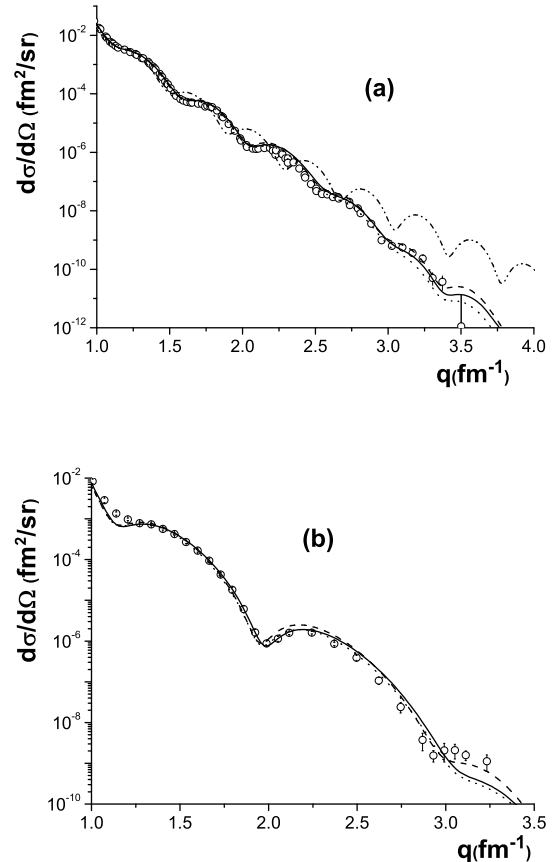


FIG. 3: Elastic electron scattering cross section in the NL3 (dashed line), TW (full line) and DDME1 (dotted line) approaches for a) ^{208}Pb and b) ^{48}Ca . E is the electron incident energy taken as 502 MeV for ^{208}Pb and as 757.5 MeV for ^{48}Ca . Experimental data are from [22] and [23] respectively. The dot-dashed line in a) corresponds to the Thomas-Fermi approximation and TW parametrization.

section for NL3 and DDH models are compared with the experimental data for ^{208}Pb and ^{48}Ca . Finite size proton as well as center-of-mass effects were also included in the cross-section calculation. In both cases the theoretical and experimental results are in very good agreement and both models show very small quantitative differences along all the momentum transfer region covered by the data. While TW and DDME1 seem to give a slightly better description for ^{208}Pb , NL3 results are closer to the cross section for ^{48}Ca at momentum transfers between 3.0 and 3.5 fm^{-1} . For the sake of completeness we have added the results obtained with the Thomas-Fermi approximation for the TW parametrization of the DDH model for ^{208}Pb . One can see that the results for the cross section start to deviate from the experimental points around 1.5 fm^{-1} with larger discrepancies at larger momentum transfers.

As for the asymmetry, our results are displayed in Fig.

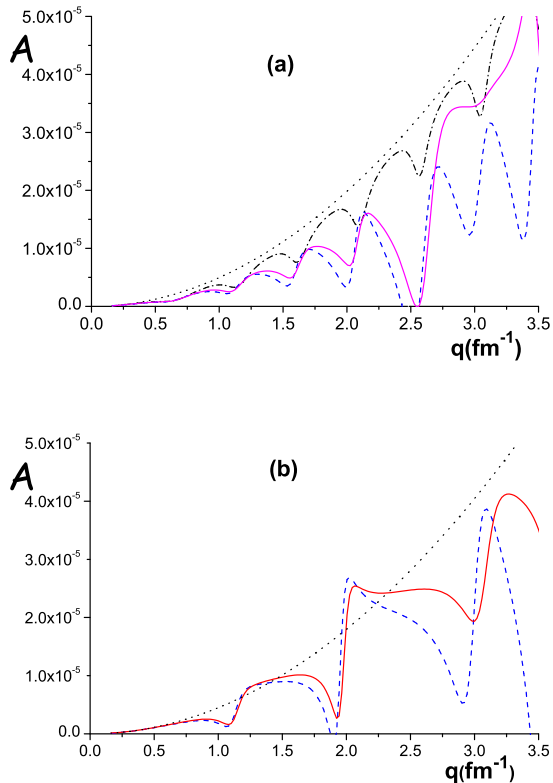


FIG. 4: Asymmetry obtained for a) ^{208}Pb and b) ^{48}Ca in the NL3 (dashed line) and TW (full line). The dotted line is the PWBA result and the dash-dotted one is the three parameter Fermi result (*Fermi3p*) as explained in the text. The incident electron energy was chosen as $E = 800\text{MeV}$.

4 for ^{208}Pb . The curve labeled PWBA is simply the result obtained from equation (23) in the Appendix, for the case where $Z \rho_n = N \rho_p$. This can be compared with the curve labeled *Fermi3p*, where the same condition is imposed but the cross-section calculation considered the partial wave expansion method and a three parameter Fermi distribution to obtain the Coulomb and weak potentials as defined in the Appendix. The difference between those curves clearly states the necessity to incorporate the electron wave distortion effects in the calculation of the asymmetry. The other two curves give us the structure effects coming from the NL3 and DDH models respectively. Similar results are shown in Fig. 4 for ^{48}Ca . One should notice that while the proton distribution in the NL3 and DDH models follow the same trend even for large momentum transfer, as can be seen from Fig. 3, the asymmetry starts to present important qualitative differences at $q \gtrsim 2\text{fm}^{-1}$, indicating that the neutron distribution seems to be more sensitive to the model used.

IV. CONCLUSIONS

In the present work we have recalculated the neutron skin thickness and the asymmetry that will be measured at the PREX experiment with two kinds of relativistic models previously used within a Thomas-Fermi plus PWBA approximations. We have here considered the full solution of the Dirac equation and used an exact calculation for the scattered electron wavefunction. Density dependent and constant coupling relativistic models provide different results and so the model dependence of the electron scattering asymmetry is confirmed by the more exact calculation, although it is still very hard to be extracted from small momentum transfer data.

If a linear relation between the neutron skin thickness and the proton-neutron asymmetry of the considered nuclei is really to be satisfied, as suggested in [14], the TW and DDME1 model parametrizations provide results within the appropriate range while the NL3 results for very asymmetric nuclei are outside the upper limit imposed by the present data.

Once a more precise measurement of the neutron skin is published, it will certainly provide a better constraint to different models and our results should then be revisited for a proper comparison.

V. APPENDIX - CROSS SECTION FOR POLARIZED ELECTRONS

The electron hadron Lagrangian density is

$$\mathcal{L} = \bar{\psi} [\gamma_\mu (i\partial^\mu + eA^\mu + \gamma_5 A_W^\mu) - m_e] \psi + \mathcal{L}_H, \quad (17)$$

where \mathcal{L}_H is the hadronic Lagrangian, A_μ is the electromagnetic field generated by the hadronic target,

$$A_W^\mu = -\frac{G}{\sqrt{2}} J^{\mu, NC}, \quad (18)$$

is the weak field and G the Fermi constant. In the elastic scattering of electrons from an even-even spherical nucleus whose *elementary* particles are just the protons and neutrons, only the static time component of the currents contribute and the electron obeys the Dirac equation:

$$[\vec{\alpha} \cdot \vec{p} + \gamma_0 m_e + V(r) + \gamma_5 V_A(r)] \psi = E \psi, \quad (19)$$

with $V(r) = -eA_0(r)$ and $V_A(r) = \frac{G}{\sqrt{2}} J_0^{NC}(r)$. From the standard model we know that the weak neutral (NC) current is [28]:

$$J^{0, NC}(r) = \chi_p \rho_p(r) + \chi_n \rho_n(r). \quad (20)$$

The above constants are $\chi_p \simeq 0.04$ and $\chi_n = -0.5$. Hence, we conclude that the weak potential depends strongly on the neutron distribution in nuclei, while the

e.m. field A_0 depends (not considering the neutron electric form factor) exclusively on the proton distribution. For high energy electrons and scattering angles not too close to 180° we may use the approximation $\frac{m_e}{E} \sim 0$, for which the Dirac equation can be rewritten in the form:

$$[\vec{\alpha} \cdot \vec{p} + V(r) \pm V_A(r)]\psi_{\pm} = E\psi_{\pm}, \quad (21)$$

with $\psi_{\pm} = \frac{1}{2}(1 \pm \gamma_5)\psi$ and the \pm signs represent the two possible electron initial polarization (helicity) states. We have solved the above equation for the electron exactly, using the well-known partial wave phase-shift expansion method, as explained, for instance in [29]. Note that for each electron helicity state, a different set of phase-shifts must be determined, whose differences come from the contribution of the weak potential. We now define the asymmetry through the expression:

$$\mathcal{A} = \frac{d\sigma_+/d\Omega - d\sigma_-/d\Omega}{d\sigma_+/d\Omega + d\sigma_-/d\Omega}, \quad (22)$$

where $d\sigma_{\pm}/d\Omega$ is the differential cross section for initially

polarized electrons with positive(+) and negative (-) helicities. The solution of equation (21) in first order perturbation theory lead us to the Plane Wave Born Approximation [12] result:

$$\mathcal{A} = -\frac{Gq^2}{2\pi\alpha\sqrt{2}}[\chi_p + \chi_n \frac{\rho_n(q)}{\rho_p(q)}], \quad (23)$$

where q is the momentum transfer and $\rho_{n(p)}(q)$ being the neutron (proton) distribution in q space. Even for medium mass nuclei, important differences between the PWBA and the exact result should be found in the asymmetry [17]. In this paper, all the cross sections were obtained through the full solution of the Dirac equation for the electron.

ACKNOWLEDGMENTS

This work was partially supported by CNPq(Brazil).

-
- [1] B. Serot and J.D. Walecka, *Advances in Nuclear Physics* 16, Plenum-Press, (1986) 1.
- [2] H. Lenske and C. Fuchs, *Phys. Lett.* **B 345**, 355 (1995); C. Fuchs, H. Lenske and H.H. Wolter, *Phys. Rev.* **C 52**, 3043 (1995).
- [3] S. Typel and H. H. Wolter, *Nucl. Phys.* **A656**, 331 (1999).
- [4] T. Gaitanos, M. Di Toro, S. Typel, V. Baran, C. Fuchs, V. Greco and H. H. Wolter, *Nucl. Phys.* **A732**, 24 (2004).
- [5] G.E. Brown and M. Rho, *Phys. Rev. Lett.* **66**, 2720 (1991).
- [6] G. A. Lalazissis, J. König and P. Ring, *Phys. Rev. C* **55**, 540 (1997).
- [7] K. Sumiyoshi, H. Kuwabara, H. Toki, *Nucl. Phys.* **A 581**, 725 (1995).
- [8] N. K. Glendenning, *Compact Stars*, Springer-Verlag, New-York, 2000.
- [9] C.J. Horowitz and J.Piekarewicz, *Phys. Rev.* **C 64**, 062802R (2001); J.K. Bunta and S. Gmuca, *Phys. Rev. C* **68**, 054318 (2003); J.K. Bunta and S. Gmuca, *Phys. Rev. C* **70**, 054309 (2004).
- [10] H. de Vries, C.W. de Jager and C. de Vries, *Atomic and Nuclear Data Tables* **36**, 495 (1987).
- [11] C.J. Horowitz, S.J. Pollock, P.A. Souder and R. Michaels, *Phys. Rev. C* **63**, 025501 (2001).
- [12] T.W. Donnelly, J. Dubach and I. Sick, *Nucl. Phys.* **A503** 589 (1989).
- [13] K.A. Aniol et al. (HAPPEX) (2005), nucl-ex/0506010; *ibidem*, nucl-ex/0506011; R. Michaels, P.A. Souder and G.M. Urciuoli (2005), URL <http://hallaweb.jlab.org/parity/prex>.
- [14] A. Trzcinska, J. Jastrzebski, P. Lubinski, F.J. Hartmann, R. Schmidt, T. von Egidy and B. Klos, *Phys. Rev. Lett.* **87**, 082501 (2001).
- [15] B. Klos et al., nucl-ex/0702016.
- [16] S.S. Avancini, J.R. Marinelli, D. P. Menezes, M.M. W. Moraes and C. Providência, *Phys. Rev. C* **75** (2007) 055805.
- [17] C.J. Horowitz, *Phys. Rev.* **C57**, 3430 (1998).
- [18] T. Niksic, D. Vretenar, P. Finelli and P. Ring, *Phys. Rev. C* **66**, 024306 (2002); D. Vretenar, T. Niksic and P. Ring, *Phys. Rev. C* **68**, 024310 (2003).
- [19] Y.K. Gambhir, P. Ring and A. Thimet, *Ann. Phys.* **198**, 132 (1990).
- [20] S.S. Avancini and D.P. Menezes, *Phys. Rev. C* **74**, 015201 (2006).
- [21] J.W. Negele, *Phys. Rev. C* **1**, 1260 (1970).
- [22] B. Frois et al., *Phys. Rev. Letters* **38**, 152 (1977).
- [23] J.B. Bellicard et al, *Phys. Rev. C* **21**, 1652 (1980).
- [24] G.Fricke, C. Bernhardt, K.Heilig, L.A. Schaller, L. Schellinberg, E.B. Shera, C.W. de Jager, *At. Data Nucl. Data Tables* **60** (1995)177.
- [25] G. Audi, A.H. Waptra, C. Thibault, *Nucl. Phys.* **A 729**, 337 (2003).
- [26] A. Krasznahorkay et al., *Nucl. Phys.* **A 731**, 224 (2004).
- [27] V.E. Starodubsky, N.M. Hintz, *Phys. Rev. C* **49**, 2118(1994).
- [28] W. Greiner and B. Muller, *Gauge Theory of the Weak Interactions* (Springer, 1996).
- [29] J. F. Prewitt and L. W. Wright, *Phys. Rev.* **C9**, 2033 (1974).
- [30] Data obtained from www.nndc.bnl.gov; visited on 11 July 2007.

TABLE I: ^{208}Pb properties

model	approximation	R_n (fm)	R_p (fm)	R_c (fm)	θ (fm)	B/A MeV	σ MeV/fm ²
NL3	TF	5.79	5.57		0.22	-7.79	0.96
NL3	Dirac	5.74	5.46	5.51	0.28	-7.91	1.13
TW	TF	5.68	5.52		0.16	-7.46	1.10
TW	Dirac	5.61	5.42	5.48	0.20	-7.78	1.30
DDME1	Dirac	5.66	5.46	5.51	0.20	-7.91	1.18
exp.[24]				5.50			
exp. [25]						-7.87	
exp. [26]					0.12 ± 0.07		
exp. [27]					0.20 ± 0.04		
exp. [15]					$0.16 \pm 0.02 \pm 0.04$		

TABLE II: Finite nuclei properties

model	nuclei	R_n (fm)	R_p (fm)	R_c (fm)	θ (fm)	B/A MeV	σ MeV/fm ²
NL3	^{40}Ca	3.32	3.37	3.43	-0.05	-8.62	1.48
TW	^{40}Ca	3.28	3.33	3.39	-0.05	-8.36	1.60
DDME1	^{40}Ca	3.32	3.37	3.43	-0.05	-8.62	1.45
exp.[18]	^{40}Ca			3.48		-8.55	
NL3	^{48}Ca	3.60	3.37	3.44	0.23	-8.72	1.54
TW	^{48}Ca	3.54	3.35	3.42	0.19	-8.49	1.70
DDME1	^{48}Ca	3.58	3.39	3.46	0.19	-8.66	1.53
exp.[30]	^{48}Ca					-8.67	
exp.[18]	^{48}Ca			3.48			
NL3	^{90}Zr	4.30	4.19	4.25	0.11	-8.86	1.37
TW	^{90}Zr	4.24	4.15	4.22	0.08	-8.55	1.52
DDME1	^{90}Zr	4.28	4.19	4.25	0.08	-8.73	1.38
exp.[30]	^{90}Zr					-8.71	
NL3	^{66}Ni	3.96	3.76	3.82	0.20	-8.74	1.47
TW	^{66}Ni	3.89	3.74	3.81	0.15	-8.56	1.63
DDME1	^{66}Ni	3.93	3.77	3.84	0.16	-8.72	1.49
exp.[30]	^{66}Ni					-8.74	